Effects of viscoelasticity on the oscillatory behavior of a two-link filament model

Sophia Nelson

UC Davis REU 2021

Abstract

A subgroup of microscopic organisms, known as swimmers, use thin rod-like structures called cilia and flagella to propel themselves in various fluid environments. This locomotion is driven by both the dynamics of intracellular molecular motors within the flagella/cilia and the hydrodynamic forces exerted on the swimmer. Swimmer gait is subject to changes in both the external and internal environments. In this work, we are interested in the 2D planar motion of a flagellum/cilium driven by a follower force applied tangentially at the tail and pinned at the head. To characterize this phenomenon, we consider a discretized, two-link filament model that exhibits oscillatory behavior. We explore this motion in three different fluid models: a viscous model, a Maxwell elastic model, and an Oldroyd-B viscoelastic model. Changes in the frequency, amplitude, and stability of the emergent oscillations were observed as a result of variations in fluid properties. This result highlights the adaptive nature of swimmers in viscoelastic environments.

1 Introduction

Many microorganisms that live in fluid environments utilize thin appendages called cilia and flagella to propel themselves through the fluid. Their pattern of swimming motion is influenced by changes in molecular motor activity within the filament, as well as the properties of the surrounding fluid. There are many aspects to consider when modeling this motion. Cilia and flagella are complex structures, comprised of microtubules that are arranged in a "bundle of straws" manner within the filament. Dynein motors are attached to the microtubules and cause the filament to bend by "walking" along the microtubules. The elastic forces that result from this bending, coupled with the forces from the surrounding fluid, is what causes the filament "beat," and ultimately propulsion through the fluid. The swimming of microorganisms occurs at what is called a low Reynolds number (*Purcell, 1976*) [2], in which the ratio of inertial forces to viscous forces is so small that inertia is negligible.

Rather than diving in to the molecular motor activity and the complex internal structure of cilia and flagella, we simplified the model to consider a tangential "follower force" that acts on the tip of the filament as it beats.

Work by *De Canio et al. (2017)*[1] has characterized this motion using the follower force model in viscous fluids. Specifically, they analyzed the motion of an elastic filament, pinned at one end, acted on by a tangential follower force at the tail within a viscous, low Reynolds number regime. We are interested in extending this framework to viscoelastic fluids, as this encompasses a wider variety of fluid properties that are relevant to biological systems.

The viscous model in section 3 replicates results from De Canio's paper, then we go on to consider how adding a viscoelastic aspect to the fluid impacts locomotion. This is is first done through the Maxwell model in section 4, which is then modified to an Oldroyd-B model, explored in section 5.

2 Two-link model

Inspired by Decanio et al., we considered a filament made of two discrete links, as shown in Figure 1.

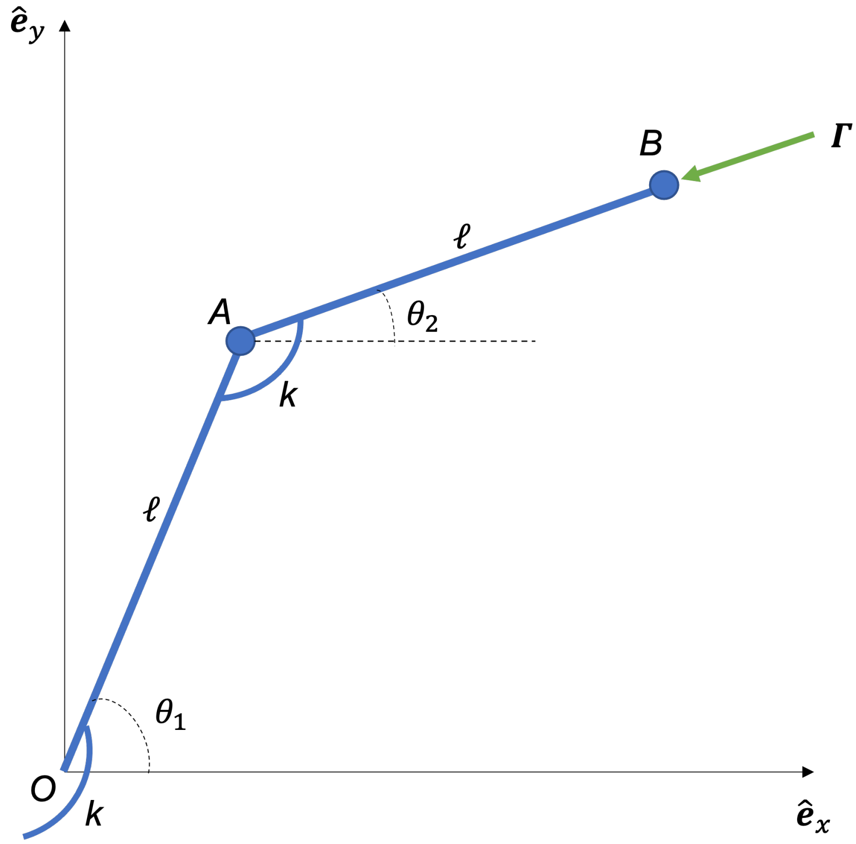

Figure 1: Two-link filament model.

The filament is clamped at point O, and is comprised of two straight rods of infinitesimal thinness, connected at point A. A tangential follower force, $\mathbf{\Gamma}$, acts at point B, which is at the tip of the filament. The filament has two torsion springs at points O and A, each with stiffness constant k.

2.1 Describing the two-link model

We denote the location of points A and B as

$$\mathbf{r}_A = A - O = l(\cos\theta_1, \sin\theta_1)$$

and

$$\mathbf{r}_B = B - O = l(\cos\theta_1 + \cos\theta_2, \sin\theta_1 + \sin\theta_2),$$

with velocities

$$\mathbf{v}_A = \dot{r}_A = l\dot{\theta}_1(-\sin\theta_1, \cos\theta_1)$$

and

$$\mathbf{v}_B = \dot{r}_B = l[\dot{\theta}_1(-\sin\theta_1, \cos\theta_1) + \dot{\theta}_2(-\sin\theta_2, \cos\theta_2).$$

The torsional spring restoring moments for the springs at θ_1 and θ_2 are $M_O = -k\theta_1$ at point O, and $M_A = -k(\theta_2 - \theta_1)$ at point A.

We can describe the follower force, $\mathbf{\Gamma}$, as $-\Gamma\hat{t}$, with magnitude $\Gamma > 0$, and direction $\hat{t} = (\cos(\theta_2), \sin(\theta_2))$ as the unit tangent vector joining A and B.

Because we are assuming that the links are infinitesimally thin, the drag forces only act at points A and B as $\mathbf{F}_A = -\zeta v_A$ and $\mathbf{F}_B = -\zeta v_B$, for some effective drag coefficient ζ.

3 Viscous model

The first model we will consider is the two-link model in a purely viscous fluid. In this model, our goal was to recreate results from *DeCanio et al.* to ensure we understood the derivation of ODEs, linear analysis, and implementation in Matlab.

3.1 Equations of motion

To derive the equations of motion for a two-link filament model in a viscous fluid, we apply the principal of virtual work:

$$\mathbf{\Gamma} \cdot \delta \mathbf{r}_B + \mathbf{F}_B \cdot \delta \mathbf{r}_B + \mathbf{F}_A \cdot \delta \mathbf{r}_A - k\theta_1 \delta\theta_1 - k(\theta_1 - \theta_2)(\delta\theta_1 - \delta\theta_2) = 0, \tag{3.1}$$

in which $\delta \mathbf{r}_A$, $\delta \mathbf{r}_B$, $\delta\theta_1$, and $\delta\theta_2$ are virtual displacements of their respective variables.

We begin by evaluating $\delta \mathbf{r}_A$ and $\delta \mathbf{r}_B$:

$$\begin{aligned}
\delta \mathbf{r}_A &= \frac{\partial \mathbf{r}_A}{\partial \theta_1}\delta\theta_1 + \frac{\partial \mathbf{r}_A}{\partial \theta_2}\delta\theta_2 \\
&= l(-\sin\theta_1, \cos\theta_1)\delta\theta_1 \\
\delta \mathbf{r}_B &= \frac{\partial \mathbf{r}_B}{\partial \theta_1}\delta\theta_1 + \frac{\partial \mathbf{r}_B}{\partial \theta_2}\delta\theta_2 \\
&= l[(-\sin\theta_1, \cos\theta_1]\delta\theta_1 + (-\sin\theta_2, \cos\theta_2)\delta\theta_2].
\end{aligned}$$

We then evaluate each term from equation 3.1 as follows:

$$\begin{aligned}
\mathbf{\Gamma} \cdot \delta \mathbf{r}_B &= -\Gamma(\cos\theta_2, \sin\theta_2) \cdot l[(-\sin\theta_1, \cos\theta_1]\delta\theta_1 + (-\sin\theta_2, \cos\theta_2)\delta\theta_2] \\
&= -\Gamma l[(-\cos\theta_2\sin\theta_1 + \sin\theta_2\cos\theta_1)\delta\theta_1 + (-\cos\theta_2\sin\theta_2 + \sin\theta_2\cos\theta_2)\delta\theta_2] \\
&= -\Gamma l[-\sin(\theta_1 - \theta_2)]\delta\theta_1 \\
&= \Gamma l[\sin(\theta_1 - \theta_2)]\delta\theta_1 \\
\mathbf{F}_B \cdot \delta \mathbf{r}_B &= -\zeta l[\dot\theta_1(-\sin\theta_1, \cos\theta_1) + \dot\theta_2(-\sin\theta_2, \cos\theta_2)] \cdot l[(-\sin\theta_1, \cos\theta_1)\delta\theta_1 + (-\sin\theta_2, \cos\theta_2)\delta\theta_2] \\
&= -\zeta l^2[(\dot\theta_1\sin^2\theta_1 + \dot\theta_2\sin\theta_2\sin\theta_1 + \dot\theta_1\cos^2\theta_1 + \dot\theta_2\cos\theta_2\cos\theta_1)\delta\theta_1 \\
&+ (\dot\theta_1\sin\theta_1\sin\theta_2 + \dot\theta_2\sin^2\theta_2 + \dot\theta_1\cos\theta_1\cos\theta_2 + \dot\theta_2\cos^2\theta_2)\delta\theta_2] \\
&= -\zeta l^2[(\dot\theta_1 + \dot\theta_2\cos(\theta_1 - \theta_2))\delta\theta_1 + (\dot\theta_2 + \dot\theta_1\cos(\theta_1 - \theta_2))\delta\theta_2] \\
\mathbf{F}_A \cdot \delta \mathbf{r}_A &= -\zeta l\dot\theta_1(-\sin\theta_1, \cos\theta_1) \cdot l(-\sin\theta_1, \cos\theta_1)\delta\theta_1 \\
&= -\zeta l^2\dot\theta_1(\sin^2\theta_1 + \cos^2\theta_1)\delta\theta_1 \\
&= -\zeta l^2\dot\theta_1\delta\theta_1
\end{aligned}$$

Applying this to equation 3.1, we have

$$\begin{aligned}
\Gamma l[\sin(\theta_1 - \theta_2)]\delta\theta_1 - \zeta l^2[(\dot\theta_1 + \dot\theta_2\cos(\theta_1 - \theta_2))\delta\theta_1 + (\dot\theta_2 + \dot\theta_1\cos(\theta_1 - \theta_2))\delta\theta_2]& \\
- \zeta l^2\dot\theta_1\delta\theta_1 - k\theta_1\delta\theta_1 - k(\theta_1 - \theta_2)(\delta\theta_1 - \delta\theta_2) &= 0
\end{aligned}$$

To nondimensionalize, we scale time as $\hat{t} = kt/\zeta l^2$ and set our parameter $\Sigma = \Gamma l/k$ as the ratio between the strength of the follower force and the spring constant of the filament, to obtain

$$\begin{aligned}
\Sigma\sin(\theta_1 - \theta_2)\delta\theta_1 - [(\dot\theta_1 + \dot\theta_2\cos(\theta_1 - \theta_2))\delta\theta_1 + (\dot\theta_2 + \dot\theta_1\cos(\theta_1 - \theta_2))\delta\theta_2]& \\
- \dot\theta_1\delta\theta_1 - \theta_1\delta\theta_1 - (\theta_2 - \theta_1)\delta\theta_2 + (\theta_2 - \theta_1)\delta\theta_1 &= 0
\end{aligned}$$

Grouping by $\delta\theta_1$ and $\delta\theta_2$, we have

$$[\Sigma \sin(\theta_1 - \theta_2) - (\dot{\theta}_1 + \dot{\theta}_2 \cos(\theta_1 - \theta_2) - \dot{\theta}_1 - \theta_1 + (\theta_2 - \theta_1)]\delta\theta_1 \\ + [-(\dot{\theta}_2 + \dot{\theta}_1 \cos(\theta_1 - \theta_2)) - (\theta_2 - \theta_1)]\delta\theta_2 = 0$$

Due to the arbitrariness of $\delta\theta_1$ and $\delta\theta_2$, we can separate this equation into the following system of ODEs:

$$\Sigma \sin(\theta_1 - \theta_2) - [2\dot{\theta}_1 + \dot{\theta}_2 \cos(\theta_1 - \theta_2)] - 2\theta_1 + \theta_2 = 0 \tag{3.2}$$

$$-\dot{\theta}_1 \cos(\theta_1 - \theta_2) - \dot{\theta}_2 + \theta_1 - \theta_2 = 0. \tag{3.3}$$

3.2 Linear stability analysis

We linearize equations 3.2 and 3.3 about a horizontal filament, in which $\theta_1 = \theta_2 = 0$. Assuming small deviations from the horizontal state, we can approximate $\sin\theta \approx \theta$ and $\cos\theta \approx 1$. This results in the linearized system

$$\Sigma(\theta_1 - \theta_2) - (2\dot{\theta}_1 + \dot{\theta}_2) - 2\theta_1 + \theta_2 = 0 \tag{3.4}$$

$$-\dot{\theta}_1 - \dot{\theta}_2 + \theta_1 - \theta_2 = 0. \tag{3.5}$$

We assume oscillatory solutions of the form $\theta_j = \hat{\theta}_j e^{\omega \hat{t}}$ to obtain

$$\Sigma(\hat{\theta}_1 - \hat{\theta}_2) - \omega(2\hat{\theta}_1 + \hat{\theta}_2) - 2\hat{\theta}_1 + \hat{\theta}_2 = 0 \tag{3.6}$$

$$-\omega(\hat{\theta}_1 + \hat{\theta}_2) + \hat{\theta}_1 - \hat{\theta}_2 = 0 \tag{3.7}$$

and form a matrix based on the coefficients of $\hat{\theta}_1$ and $\hat{\theta}_1$:

$$\begin{bmatrix} \Sigma - 2\omega - 2 & -\Sigma - \omega + 1 \\ -\omega + 1 & -\omega - 1 \end{bmatrix}. \tag{3.8}$$

Setting the determinant of this matrix equal to zero, we can solve for the nontrivial eigenvalues of the system:

$$\omega^2 + 2\omega(3 - \Sigma) + 1 = 0,$$

resulting in the eigenvalue solutions

$$\omega_{\pm} = \Sigma - 3 \pm \sqrt{(\Sigma - 4)(\Sigma - 2)}.$$

The eigenvalues for this system are plotted in Figure 2. The real part of the eigenvalues correspond to the growth rate of oscillations, while the imaginary part corresponds to the frequency of oscillations.

From this, we can predict the stability of the nonlinear system for varying Σ values on a case-by-case basis.

1. $\Sigma \leq 2 \Rightarrow \omega_{\pm} < 0$, so the system is stable, with no oscillations.
2. $2 < \Sigma < 3 \Rightarrow \mathrm{Re}(\omega) < 0$ and $\mathrm{Im}(\omega) \neq 0$, so the system is stable, with decaying oscillations.
3. $\Sigma = 3 \Rightarrow \mathrm{Re}(\omega) = 0$ and $\mathrm{Im}(\omega) \neq 0$, so the system is stable, with constant amplitude oscillations.
4. $3 < \Sigma < 4 \Rightarrow \mathrm{Re}(\omega) > 0$ and $\mathrm{Im}(\omega) \neq 0$, so the system is unstable, with exponentially growing oscillations.
5. $\Sigma \geq 4 \Rightarrow \omega_{\pm} > 0$, so the system is unstable, and θ_1 and θ_2 diverge.

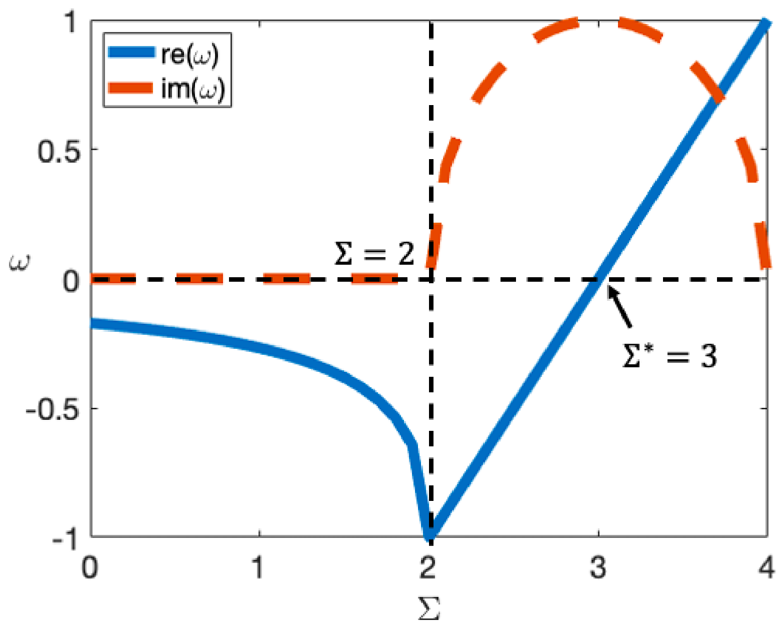

Figure 2: Maximum real part of the eigenvalues from the linear system of the viscous two-link model and its corresponding imaginary part. Real part corresponds to the growth rate of oscillations, imaginary part corresponds to oscillatory frequency.

The Σ^* value in Figure 2 is the Hopf bifurcation point of this system, which occurs at $\Sigma = 3$, when real part of the eigenvalue is zero. This is the point at which the system changes stability, switching from a stable system with exponentially decaying oscillations to an unstable system with exponentially growing oscillations. From a biological perspective, this is the point at which the magnitude of the follower force is large enough to cause the filament to buckle, resulting in sustained oscillations.

3.3 Solution to nonlinear system

We return to the nonlinear system, equations 3.2 and 3.3. We solve this system in Matlab using the ode45 solver, as show in Figure 3.

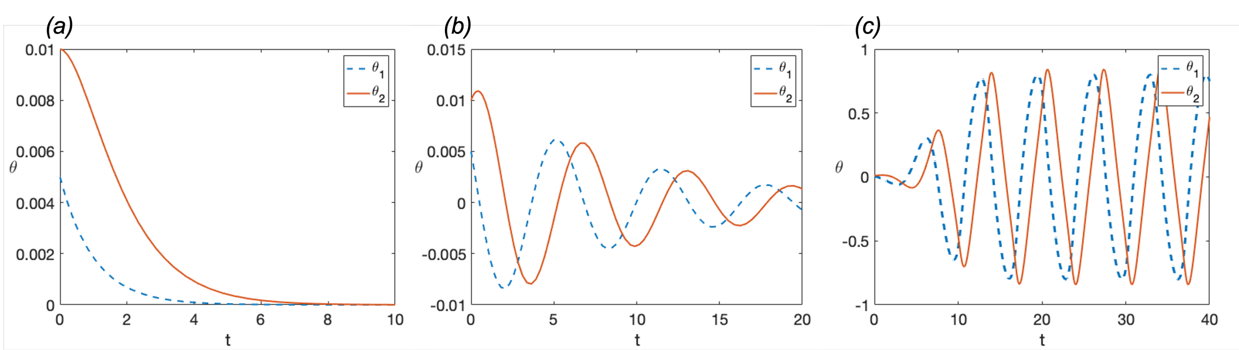

Figure 3: Change in θ_1 and θ_2 for a viscous two-link filament model. (a) $\Sigma = 2$; (b) $\Sigma = 2.9$; (c) $\Sigma = 3.5$.

These results are consistent with our predictions from the linear stability analysis. In Figure 3(a), we see immediate filament relaxation without oscillations, in Figure 3(b), we see decaying oscillations, and in Figure 3(c), we see sustained, exponentially growing oscillations.

4 Maxwell model

Our previous model considered swimmer motion in a purely viscous fluid, such as water, but many fluid environments are viscoelastic, meaning they have an elastic component to them as well. For instance, sperm that swim in mucus live in a viscoelastic fluid [3]. Thus our next two models consider a two-link filament model in a viscoelastic fluid, allowing us to examine how viscoelasticity affects filament dynamics.

Viscoelastic fluids have both fluid and solid properties. The viscous component is a fluid property, which is a measure of resistance to flow, and the elastic component is a solid property, which is the ability to resume shape after deformation. While a viscous fluid exhibits a linear relationship between stress (σ) and strain (ϵ), we see a nonlinear relationship between the two in a viscoelastic fluid, in which stress is a function of strain and strain rate: $\sigma = \sigma(\epsilon, \dot{\epsilon})$.

Because viscoelastic fluids have fluid and solid properties, we can model them as an arrangement of springs (representing the solid, elastic component) and dashpots (representing the fluid, viscous component).

4.1 Representing the Maxwell model

The first such model we will consider is the Maxwell model. In this model, we represent a viscoelastic fluid by a linear arrangement of a spring and dashpot, as shown in Figure 4.

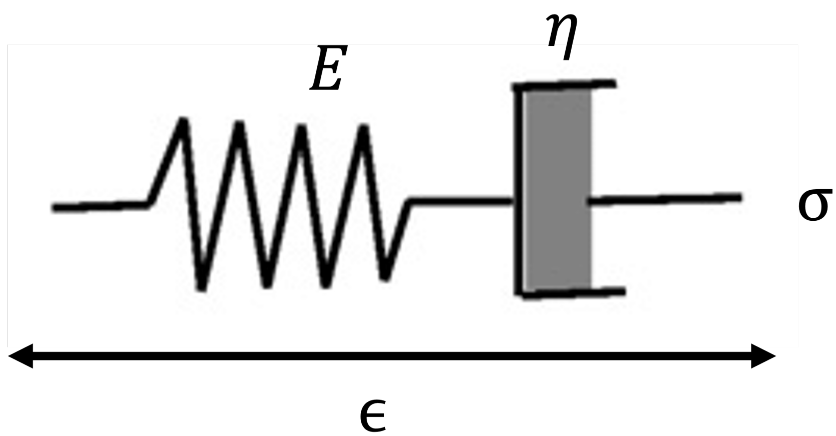

Figure 4: Maxwell model of a viscoelastic fluid. Spring has elastic modulus E, dashpot has viscosity η. The model has total stress σ and strain ϵ.

Because of the linear arrangement of this model, stress is equal throughout. Therefore, the stress on the spring is equal to the stress on the dashpot, which is equal to the total stress ($\sigma_s = \sigma_d = \sigma$). On the contrary, strain is additive, so $\epsilon_s + \epsilon_d = \epsilon$.

These relationships result in the following ODE that describes a Maxwell fluid.

$$\eta\dot{\sigma} + E\sigma = E\eta\dot{\epsilon} \tag{4.1}$$

4.2 Equations of motion

To derive the equations of motion for the Maxwell model, we will again apply the principal of virtual work (equation 3.1) but we will consider a viscoelastic force on points A and B instead of a simply viscous force. Recalling equation 4.1, note that the term $\eta\dot{\epsilon}$ represents viscous stress, so we will denote $\mathbf{F}_{viscous} = \eta\dot{\epsilon}$. Moreover, note that the ratio between the elastic modulus and viscosity is the fluid relaxation time, so we set $\frac{E}{\eta} = \lambda$. Manipulation of equation 4.1 results in the following:

$$\lambda\dot{\sigma} + \sigma = \mathbf{F}_{viscous}.$$

In our equations of motion for the viscous model, we denoted the viscous drag force on points A and B as $\mathbf{F}_A = -\zeta \mathbf{v}_A$ and $\mathbf{F}_B = -\zeta \mathbf{v}_B$, respectfully. Replacing $\mathbf{F}_A$ and $\mathbf{F}_B$ with the viscous stress, $\mathbf{F}_{viscous}$, which we derived from the Maxwell model, we obtain

$$-\zeta \mathbf{v}_A = \lambda \dot{\sigma}_A + \sigma_A$$

and

$$-\zeta \mathbf{v}_B = \lambda \dot{\sigma}_B + \sigma_B.$$

We replace the drag forces from our viscous equations with σ_A and σ_B, which are vectors that represent the stress on points A and B, respectively. This results in the following equations of motion

$$\begin{aligned}
\boldsymbol{\Gamma} \cdot \delta \mathbf{r}_B + \boldsymbol{\sigma}_B \cdot \delta \mathbf{r}_B + \boldsymbol{\sigma}_A \cdot \delta \mathbf{r}_A - k\theta_1 \delta\theta_1 - k(\theta_1 - \theta_2)(\delta\theta_1 - \delta\theta_2) = 0 && (4.2)\\
\lambda \dot{\boldsymbol{\sigma}}_A + \boldsymbol{\sigma}_A = -\zeta \mathbf{v}_A && (4.3)\\
\lambda \dot{\boldsymbol{\sigma}}_B + \boldsymbol{\sigma}_B = -\zeta \mathbf{v}_B. && (4.4)
\end{aligned}$$

Thinking of σ_A and σ_B component-wise as $\sigma_A = (\sigma_{A_x}, \sigma_{A_y})$ and $\sigma_B = (\sigma_{B_x}, \sigma_{B_y})$, and evaluating equation 4.2, we obtain the differential algebraic equation (DAE) system

$$\begin{aligned}
& -\Gamma l \sin(\theta_2 - \theta_1) + l\big[-(\sigma_{A_x} + \sigma_{B_x})\sin\theta_1 + \big(\sigma_{A_y} + \sigma_{B_y}\big)\cos\theta_1\big] + k(\theta_2 - 2\theta_1) = 0 && (4.5)\\
& l\big[-\sigma_{B_x}\sin\theta_2 + \sigma_{B_y}\cos\theta_2\big] - k(\theta_2 - \theta_1) = 0 && (4.6)\\
& \lambda\dot{\sigma}_{A_x} + \sigma_{A_x} = \zeta l \dot{\theta}_1 \sin\theta_1 && (4.7)\\
& \lambda\dot{\sigma}_{A_y} + \sigma_{A_y} = -\zeta l \dot{\theta}_1 \cos\theta_1 && (4.8)\\
& \lambda\dot{\sigma}_{B_x} + \sigma_{B_x} = \zeta l \Big(\dot{\theta}_1 \sin\theta_1 + \dot{\theta}_2 \sin\theta_2\Big) && (4.9)\\
& \lambda\dot{\sigma}_{B_y} + \sigma_{B_y} = -\zeta l \Big(\dot{\theta}_1 \cos\theta_1 + \dot{\theta}_2 \cos\theta_2\Big), && (4.10)
\end{aligned}$$

in which equations 4.5 and 4.6 are mechanical constraints.

4.3 Linearization

We linearize our DAE system as we did in the viscous model, about a horizontal filament in which $\theta_1 = \theta_2 = 0$. This results in the linear system

$$\begin{aligned}
& -\Gamma l(\theta_2 - \theta_1) + l(\sigma_{A_x} + \sigma_{B_x}) + k(\theta_2 - 2\theta_1) = 0 && (4.11)\\
& l\sigma_{B_y} - k(\theta_2 - \theta_1) = 0 && (4.12)\\
& \lambda\dot{\sigma}_{A_x} + \sigma_{A_x} = 0 && (4.13)\\
& \lambda\dot{\sigma}_{A_y} + \sigma_{A_y} = -\zeta l \dot{\theta}_1 && (4.14)\\
& \lambda\dot{\sigma}_{B_x} + \sigma_{B_x} = 0 && (4.15)\\
& \lambda\dot{\sigma}_{B_y} + \sigma_{B_y} = -\zeta l \Big(\dot{\theta}_1 + \dot{\theta}_2\Big) && (4.16)\\
& && (4.17)
\end{aligned}$$

Note that equations 4.13 and 4.15 represent exponential decay, so the x-components of our stress vectors are negligible in our linear system. Therefore, our linear system is

$$\begin{aligned}
& -\Gamma l(\theta_2 - \theta_1) + l(\sigma_{A_x} + \sigma_{B_x}) + k(\theta_2 - 2\theta_1) = 0\\
& l\sigma_{B_y} - k(\theta_2 - \theta_1) = 0\\
& \lambda\dot{\sigma}_{A_y} + \sigma_{A_y} = -\zeta l \dot{\theta}_1\\
& \lambda\dot{\sigma}_{B_y} + \sigma_{B_y} = -\zeta l \Big(\dot{\theta}_1 + \dot{\theta}_2\Big)
\end{aligned}$$

4.4 Nondimensionalization

We nondimensionalize the linear system by scaling t, σ, and θ using the substitutions $t = T\hat{t}$, $\sigma = \tilde{\Sigma}\hat{\sigma}$, and $\theta = \alpha\hat{\theta}$, for some scaling factors T, $\tilde{\Sigma}$, and α.

Making these substitutions, we obtain

$$-\Gamma l\alpha(\hat{\theta}_2 - \hat{\theta}_1) + l\tilde{\Sigma}(\hat{\sigma}_{A_y} + \hat{\sigma}_{B_y}) + k\alpha(\hat{\theta}_1 - 2\hat{\theta}_2) = 0 \tag{4.18}$$

$$l\tilde{\Sigma}\hat{\sigma}_{B_y} - k\alpha(\hat{\theta}_2 - \hat{\theta}_1) = 0 \tag{4.19}$$

$$\lambda\tilde{\Sigma}\frac{1}{T}\dot{\hat{\sigma}}_{A_y} + \tilde{\Sigma}\hat{\sigma}_{A_y} = -\zeta l\alpha\frac{1}{T}\dot{\hat{\theta}}_1 \tag{4.20}$$

$$\lambda\tilde{\Sigma}\frac{1}{T}\dot{\hat{\sigma}}_{B_y} + \tilde{\Sigma}\hat{\sigma}_{B_y} = -\zeta l\alpha\frac{1}{T}(\dot{\hat{\theta}}_1 + \dot{\hat{\theta}}_2) \tag{4.21}$$

Note that the parameters of interest are related to the follower force, Γ, and the fluid relaxation time, λ. Dividing by $k\alpha$ in equations 4.18 and 4.19 allows us to relate the strength of the follower force to the strength of the springs at θ_1 and θ_2, as was done in the De Canio paper. Likewise, dividing by $\tilde{\Sigma}$ in equations 4.20 and 4.21 allows us to relate the fluid relaxation time, λ, to the mechanical relaxation time, T.

Dividing by respective scaling factors results in the following system

$$\begin{aligned}
&-\frac{\Gamma l}{k}(\hat{\theta}_2 - \hat{\theta}_1) + \frac{l\tilde{\Sigma}}{k\alpha}(\hat{\sigma}_{A_y} + \hat{\sigma}_{B_y}) + (\hat{\theta}_1 - 2\hat{\theta}_2) = 0 \\
&\frac{l\tilde{\Sigma}}{k\alpha}\hat{\sigma}_{B_y} - (\hat{\theta}_2 - \hat{\theta}_1) = 0 \\
&\lambda\frac{1}{T}\dot{\hat{\sigma}}_{A_y} + \hat{\sigma}_{A_y} = -\frac{\zeta l\alpha}{\tilde{\Sigma}}\frac{1}{T}\dot{\hat{\theta}}_1 \\
&\lambda\frac{1}{T}\dot{\hat{\sigma}}_{B_y} + \hat{\sigma}_{B_y} = -\frac{\zeta l\alpha}{\tilde{\Sigma}}\frac{1}{T}(\dot{\hat{\theta}}_1 + \dot{\hat{\theta}}_2)
\end{aligned}$$

Setting $\tilde{\Sigma} = \frac{k\alpha}{l}$ results in the cancelling out of respective coefficients in the first two equations. We have a choice to either express T in terms of λ, or as $\frac{\zeta l^2}{k}$. Being that we are interested in a parameter that relates to the fluid relaxation time, we want to be able to freely manipulate λ. Therefore, we choose $T = \frac{\zeta l^2}{k}$. Setting our parameters, we have

$$\Sigma = \frac{\Gamma l}{k},$$

which is the ratio between follower force strength and the spring constant of the filament, and

$$\Lambda = \frac{k\lambda}{\zeta l^2} = \frac{\lambda}{T},$$

which is the ratio between fluid relaxation time and mechanical relaxation time. We obtain

$$\begin{aligned}
&\Sigma(\theta_1 - \theta_2) + \sigma_{A_y} + \sigma_{B_y} + \theta_1 - 2\theta_2 = 0 \\
&\sigma_{B_y} - (\theta_2 - \theta_1) = 0 \\
&\Lambda\dot{\sigma}_{A_y} + \sigma_{A_y} = -\dot{\theta}_1 \\
&\Lambda\dot{\sigma}_{B_y} + \sigma_{B_y} = -\dot{\theta}_1 - \dot{\theta}_2
\end{aligned}$$

as our nondimensionalized linear system.

4.5 Linear stability analysis

We assume oscillatory solutions of the form $\theta_j = \hat{\theta}_j e^{\omega \hat{t}}$ and $\sigma = \hat{\sigma} e^{\sigma \hat{t}}$ to obtain

$$\begin{aligned}
&\Sigma(\hat{\theta}_1 - \hat{\theta}_2) + \hat{\sigma}_{A_y} + \hat{\sigma}_{B_y} + \hat{\theta}_1 - 2\hat{\theta}_2 = 0 \\
&\hat{\sigma}_{B_y} - (\hat{\theta}_2 - \hat{\theta}_1) = 0 \\
&\Lambda\omega\hat{\sigma}_{A_y} + \hat{\sigma}_{A_y} = -\omega\hat{\theta}_1 \\
&\Lambda\omega\hat{\sigma}_{B_y} + \hat{\sigma}_{B_y} = -\omega\hat{\theta}_1 - \omega\hat{\theta}_2
\end{aligned}$$

We form a matrix based on the coefficients of $\hat{\theta}_1$, $\hat{\theta}_1$, $\hat{\sigma}_{A_y}$, and $\hat{\sigma}_{A_y}$.

$$\begin{bmatrix} \Sigma - 2 & -\Sigma + 1 & 1 & 1 \\ 1 & -1 & 0 & 1 \\ \omega & 0 & \Lambda\omega + 1 & 0 \\ \omega & \omega & 0 & \Lambda\omega + 1 \end{bmatrix} \tag{4.22}$$

Setting the determinant of this matrix equal to zero, we can solve for the nontrivial eigenvalues of the system, as we did in for the viscous model. This results in the eigenvalue solutions

$$\omega_{\pm} = \frac{\Sigma - \Lambda - 3 \pm \sqrt{(\Sigma - 4)(\Sigma - 2)}}{-2\Sigma\Lambda + \Lambda^2 + 6\Lambda + 1}. \tag{4.23}$$

Recall that the Hopf bifurcation occurs when the real part of the eigenvalue is equal to zero. Note that because this system depends on two parameters, Λ and Σ, we expect a Hopf bifurcation curve, as opposed to the Hopf bifurcation point that we saw in the viscous system.

The real part of $\omega_{\pm}$ is zero when $\Sigma - \Lambda - 3 = 0$ and $2 \leq \Sigma \leq 4$, so our Hopf bifurcation curve for this system is $\Sigma = \Lambda + 3$. Since Λ must be positive, our bounds for this curve are $0 \leq \Lambda \leq 1$ and $3 \leq \Sigma \leq 4$.

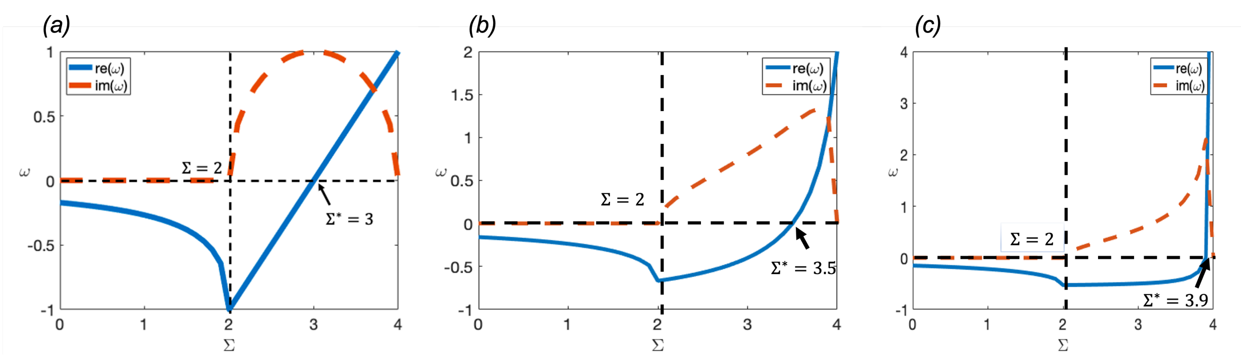

Figure 5: Real and imaginary parts of the eigenvalues for the Maxwell model system. Real part corresponds to oscillation growth, imaginary part corresponds to oscillation frequency. (a) $\Lambda = 0 \Rightarrow \Sigma^* = 3$; (b) $\Lambda = 0.5 \Rightarrow \Sigma^* = 3.5$; (c) $\Lambda = 0.9 \Rightarrow \Sigma^* = 3.9$.

We see this linear relationship between Λ and Σ^* in Figure 5. Note that when $\Lambda = 0$, we see the same results as we did in the viscous model. This is as we would expect because Λ relates to the fluid relaxation time of our viscoelastic fluid. As Λ increases, the fluid becomes more elastic. When $\Lambda = 0$, there is no elasticity involved in the fluid, it is simply viscous.

4.6 Nonlinear equations of motion

We return to our nonlinear DAE system, equations 4.5-4.10. Applying the same scaling factors as we did in the linear system, we obtain the following nondimensionalized nonlinear DAE system:

$$\Lambda\dot{\sigma}_{A_x} - \dot{\theta}_1 \sin\theta_1 = -\sigma_{A_x} \tag{4.24}$$

$$\Lambda\dot{\sigma}_{A_y} + \dot{\theta}_1 \cos\theta_1 = -\sigma_{A_y} \tag{4.25}$$

$$\Lambda\dot{\sigma}_{B_x} - \dot{\theta}_1 \sin\theta_1 - \dot{\theta}_2 \sin\theta_2 = -\sigma_{B_x} \tag{4.26}$$

$$\Lambda\dot{\sigma}_{B_y} + \dot{\theta}_1 \cos\theta_1 + \dot{\theta}_2 \cos\theta_2 = -\sigma_{B_y} \tag{4.27}$$

$$-\Sigma\sin(\theta_2-\theta_1) - (\sigma_{A_x}+\sigma_{B_x})\sin\theta_1 + (\sigma_{A_y}+\sigma_{B_y})\cos\theta_1 + \theta_2 - 2\theta_1 = 0 \tag{4.28}$$

$$-\sigma_{B_x}\sin\theta_2 + \sigma_{B_y}\cos\theta_2 - \theta_2 + \theta_1 = 0. \tag{4.29}$$

Because we are working with a DAE system, we are not able to solve this system with Matlab's ode45 solver. We turn to the DAE solver, ode15s. To input this system into ode15s, we have to find a mass matrix, M, such that $My' = F(y,t)$. Thus we transform the nonlinear system into the matrix equation

$$\begin{bmatrix} \Lambda & 0 & 0 & 0 & -\sin\theta_1 & 0 \\ 0 & \Lambda & 0 & 0 & \cos\theta_1 & 0 \\ 0 & 0 & \Lambda & 0 & -\sin\theta_1 & -\sin\theta_2 \\ 0 & 0 & 0 & \Lambda & \cos\theta_1 & \cos\theta_2 \\ 0 & 0 & 0 & 0 & 0 & 0 \\ 0 & 0 & 0 & 0 & 0 & 0 \end{bmatrix} \begin{bmatrix} \dot{\sigma}_{A_x} \\ \dot{\sigma}_{A_y} \\ \dot{\sigma}_{B_x} \\ \dot{\sigma}_{B_y} \\ \dot{\theta}_1 \\ \dot{\theta}_2 \end{bmatrix} = \begin{bmatrix} -\sigma_{A_x} \\ -\sigma_{A_y} \\ -\sigma_{B_x} \\ -\sigma_{B_y} \\ F_1 \\ F_2 \end{bmatrix}, \tag{4.30}$$

so that F_1 and F_2 are the left hand sides of equations 4.28 and 4.29, respectively, and the M is the leftmost matrix.

The solution to this system is show in Figure 6. When $\Lambda = 0$, we recover the viscous model, as we would expect. For a viscoelastic fluid, when $\Lambda = 0.5$, we see a shift in the pattern of oscillations. At $\Sigma = 2$, the filament takes longer to relax than it does in the viscous model. At $\Sigma = 2.9$, we see a slight transience before relaxation, as opposed to decaying oscillations in the viscous model. At $\Sigma = 3.3$, we see decaying oscillations instead of the growing oscillations observed in the viscous model.

Figure 7 shows how increasing viscoelasticity dampens filament oscillations for a fixed follower force. We see that increasing the fluid relaxation time stabilizes the filament. Figure 7(a) shows the filament in a purely viscous fluid, in which the oscillations exponentially grow, while 7(b) and (c) show the filament in a viscoelastic fluid, in which the filament relaxes to resting state.

4.7 Issues with Maxwell model

As with any model, the Maxwell model has its limitations. The model breaks down past certain Σ values, so we aren't able to explore what happens for high follower force strengths.

As opposed to our viscous model, which simulates a purely viscous fluid, this model simulates a purely viscoelastic fluid. We want a way to smoothly transition between the two. In order to accomplish this, we considered a new model.

5 Oldroyd-B model

The Oldroyd-B Model is another way of representing a viscoelastic fluid, and it provides a way for us to smoothly transition between a purely viscous and purely viscoelastic fluid, as seen in the Maxwell model.

Complex fluids have a total viscosity that is comprised of a fluid viscosity and a polymer viscosity. The Maxwell model only considered the polymer viscosity, so we will add the fluid viscous term to our model. We will use ζ_f as the drag coefficient for fluid viscosity, and ζ_p for polymer viscosity.

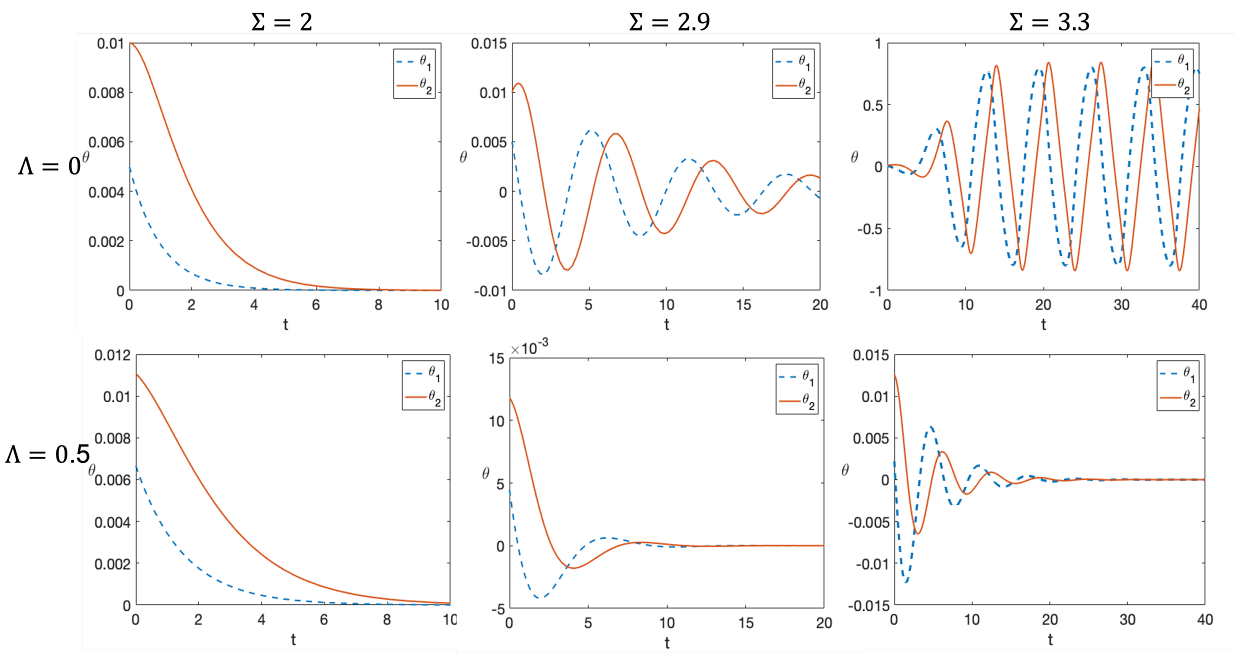

Figure 6: Change in θ_1 and θ_2 for a viscoelastic, Maxwell two-link filament model for varying values of Λ and Σ.

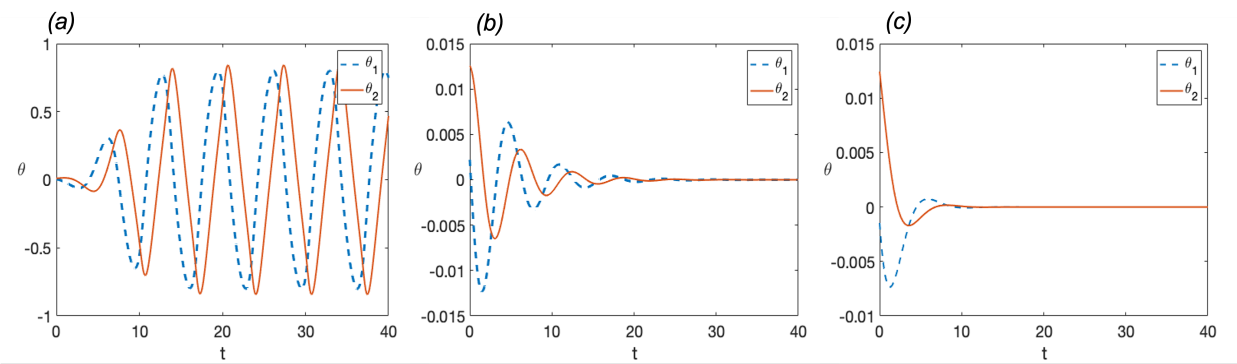

Figure 7: Change in θ_1 and θ_2 for a viscoelastic, Maxwell two-link filament model with a fixed follower force ($\Sigma = 3.3$). (a) $\Lambda = 0$; (b) $\Lambda = 0.5$; (c) $\Lambda = 1$.

5.1 Equations of motion

We modify equations 4.2 to 4.4 of the Maxwell model to include the fluid viscous term, as such:

$$\mathbf{\Gamma} \cdot \delta \mathbf{r}_B + \mathbf{F}_B \cdot \delta \mathbf{r}_B + \boldsymbol{\sigma}_B \cdot \delta \mathbf{r}_B + \mathbf{F}_A \cdot \delta \mathbf{r}_A + \boldsymbol{\sigma}_A \cdot \delta \mathbf{r}_A - k\theta_1 \delta\theta_1 - k(\theta_1 - \theta_2)(\delta\theta_1 - \delta\theta_2) = 0 \tag{5.1}$$

$$\lambda \dot{\boldsymbol{\sigma}}_A + \boldsymbol{\sigma}_A = -\zeta_p \mathbf{v}_A \tag{5.2}$$

$$\lambda \dot{\boldsymbol{\sigma}}_B + \boldsymbol{\sigma}_B = -\zeta_p \mathbf{v}_B. \tag{5.3}$$

Expanding, and treating σ component-wise results in the following nonlinear system of equations:

$$0 = -\Gamma l \sin(\theta_2 - \theta_1) + l(-\sin\theta_1(\sigma_{A_x} + \sigma_{B_x}) + \cos\theta_1(\sigma_{A_y} + \sigma_{B_y})) - 2\zeta_f l^2 \dot{\theta}_1 - \zeta_f l^2 \dot{\theta}_2 \cos(\theta_1 - \theta_2) - 2k\theta_1 + k\theta_2 \tag{5.4}$$

$$0 = l(-\sin\theta_2 \sigma_{B_x} + \cos\theta_2 \sigma_{B_y}) - \zeta_f l^2(\dot{\theta}_2 + \dot{\theta}_1 \cos(\theta_1 - \theta_2)) - k(\theta_2 - \theta_1) \tag{5.5}$$

$$\lambda \dot{\sigma}_{A_x} + \sigma_{A_x} = \zeta_p l \dot{\theta}_1 \sin\theta_1 \tag{5.6}$$

$$\lambda \dot{\sigma}_{A_y} + \sigma_{A_y} = -\zeta_p l \dot{\theta}_1 \cos\theta_1 \tag{5.7}$$

$$\lambda \dot{\sigma}_{B_x} + \sigma_{B_x} = \zeta_p l \Big(\dot{\theta}_1 \sin\theta_1 + \dot{\theta}_2 \sin\theta_2 \Big) \tag{5.8}$$

$$\lambda \dot{\sigma}_{B_y} + \sigma_{B_y} = -\zeta_p l \Big(\dot{\theta}_1 \cos\theta_1 + \dot{\theta}_2 \cos\theta_2 \Big). \tag{5.9}$$

5.2 Linearization

We linearize as we have done previously, about a horizontal filament in which $\theta_1 = \theta_2 = 0$. Similarly to the Maxwell model, the x-components of the stress vectors are negligible in the linear regime, so we obtain the following linear system:

$$0 = -\Gamma l(\theta_2 - \theta_1) + l(\sigma_{A_y} + \sigma_{B_y}) - 2\zeta_p l^2 \dot{\theta}_1 - \zeta_p l^2 \dot{\theta}_2 + k(\theta_2 - 2\theta_1) \tag{5.10}$$

$$0 = l\sigma_{B_y} - \zeta_p l^2(\dot{\theta}_2 + \dot{\theta}_1) - k(\theta_2 - \theta_1) \tag{5.11}$$

$$\lambda \dot{\sigma}_{A_y} + \sigma_{A_y} = -\zeta_p l \dot{\theta}_1 \tag{5.12}$$

$$\lambda \dot{\sigma}_{B_y} + \sigma_{B_y} = -\zeta_p l \Big(\dot{\theta}_1 + \dot{\theta}_2 \Big). \tag{5.13}$$

$$\tag{5.14}$$

5.3 Nondimensionalization

We nondimensionalize our linear system by using the scaling factors $t = T\hat{t}$, $\sigma = \tilde{\Sigma}\hat{\sigma}$, and $\theta = \alpha\hat{\theta}$:

$$0 = -\Gamma l \alpha(\hat{\theta}_2 - \hat{\theta}_1) + l\tilde{\Sigma}(\hat{\sigma}_{A_y} + \hat{\sigma}_{B_y}) - 2\frac{\zeta_p l^2 \alpha}{T}\dot{\hat{\theta}}_1 - \frac{\zeta_p l^2 \alpha}{T}\dot{\hat{\theta}}_2 + k\alpha(\hat{\theta}_2 - 2\hat{\theta}_1) \tag{5.15}$$

$$0 = l\tilde{\Sigma}\hat{\sigma}_{B_y} - \frac{\zeta_p l^2 \alpha}{T}(\dot{\hat{\theta}}_2 + \dot{\hat{\theta}}_1) - k\alpha(\hat{\theta}_2 - \hat{\theta}_1) \tag{5.16}$$

$$\frac{\lambda\tilde{\Sigma}}{T}\dot{\hat{\sigma}}_{A_y} + \tilde{\Sigma}\hat{\sigma}_{A_y} = -\frac{\zeta_p l \alpha}{T}\dot{\hat{\theta}}_1 \tag{5.17}$$

$$\frac{\lambda\tilde{\Sigma}}{T}\dot{\hat{\sigma}}_{B_y} + \tilde{\Sigma}\hat{\sigma}_{B_y} = -\frac{\zeta_p l \alpha}{T}(\dot{\hat{\theta}}_1 + \dot{\hat{\theta}}_2). \tag{5.18}$$

$$\tag{5.19}$$

As was done in the previous models, we define Σ as $\frac{\Gamma l}{k}$, so that we have a relationship between follower force strength and the spring constant. Since we added a new fluid viscosity term to this model, we need a new parameter. We want to be able to smoothly transition from the case in which there is only fluid viscosity (no polymer viscosity) to the case in which there is only polymer viscosity. To achieve this, we set our new parameter as

$$\beta = \frac{\zeta_p}{\zeta_p + \zeta_f},$$

so that it is the ratio between polymer viscosity and total viscosity. Note that with this way of defining β, we recover the viscous model when $\beta = 0$ and the Maxwell model when $\beta = 1$. Moreover, scaling time with respect to both fluid and polymer viscosity, results in $T = \frac{(\zeta_f + \zeta_p)l^2}{k}$. We define Λ as we did in the Maxwell model, as a ratio between fluid relaxation time and mechanical relaxation time, so that $\Lambda = \frac{k\lambda}{(\zeta_f + \zeta_p)l^2} = \frac{\lambda}{T}$. Applying these substitutions, we obtain the nondimensional linear system:

$$0 = \Sigma(\theta_1 - \theta_2) + \sigma_{A_y} + \sigma_{B_y} - 2(1-\beta)\dot{\theta}_1 - (1-\beta)\dot{\theta}_2 + \theta_2 - 2\theta_1 \tag{5.20}$$

$$0 = \sigma_{B_y} - (1-\beta)(\dot{\theta}_2 + \dot{\theta}_1) - \theta_2 + \theta_1 \tag{5.21}$$

$$\Lambda\dot{\sigma}_{A_y} + \sigma_{A_y} = -\beta\dot{\theta}_1 \tag{5.22}$$

$$\Lambda\dot{\sigma}_{B_y} + \sigma_{B_y} = -\beta(\dot{\theta}_1 + \dot{\theta}_2). \tag{5.23}$$

(5.24)

5.4 Linear Stability Analysis

As was done in the previous models, we assume oscillatory solutions of the form $\theta_j = \hat{\theta}_j e^{\omega\hat{t}}$ and $\sigma = \hat{\sigma} e^{\sigma\hat{t}}$ to obtain

$$\begin{aligned}
&\Sigma(\hat{\theta}_1 - \hat{\theta}_2) + \hat{\sigma}_{A_y} - \omega(1-\beta)(2\hat{\theta}_1 + \hat{\theta}_2 - 2\hat{\theta}_1) = 0 \\
&\hat{\sigma}_B - \omega(1-\beta)(\hat{\theta}_2 + \hat{\theta}_1) - \hat{\theta}_2 + \hat{\theta}_1 = 0 \\
&\omega\Lambda\hat{\sigma}_{A_y} + \hat{\sigma}_{A_y} + \omega\beta\hat{\theta}_1 = 0 \\
&\omega\Lambda\hat{\sigma}_{B_y} + \hat{\sigma}_{B_y} + \omega\beta(\hat{\theta}_1 + \hat{\theta}_2) = 0.
\end{aligned}$$

We form a matrix based off of the coefficients of this system:

$$\begin{bmatrix}
\Sigma - 2\omega(1-\beta) - 2 & -\Sigma - \omega(1-\beta) + 1 & 1 & 1 \\
-\omega(1-\beta) + 1 & -\omega(1-\beta) - 1 & 0 & 1 \\
\omega\beta & 0 & \omega\Lambda + 1 & 0 \\
\omega\beta & \omega\beta & 0 & \Lambda\omega + 1
\end{bmatrix}.$$

Solving for the zeros of the determinant numerically gives the Hopf bifurcation curves for different polymer viscosity ratios (Figure 8). The left of each curve is when we have a stable system with decaying oscillations and the right is the unstable regime associated with emergent oscillations. The leftmost curve is the case when $\beta = 0$, when we have no polymer viscosity, recovering the viscous model. Note that as we saw in the viscous model, the bifurcation point remains constant at $\Sigma = 3$. The rightmost curve represents a polymer viscosity ratio approaching 1, in which we have no fluid viscosity, recovering the Maxwell model. As we saw in the Maxwell model, there is a linear relationship between Σ and Λ for $3 \le \Sigma \le 4$. The middle curve represents an intermediate case, in which there is a $\frac{2}{3}$ ratio of polymer viscosity to total viscosity. This case is overlain with frequency prediction from the linear analysis in Figure 8(b). Note that for Σ values of approximately 3 to 3.5, a vertical slice results in two bifurcation points. This is evident in Figure 8(c), in which Figure 8(b) is restricted to $\Sigma \ge 3.25$. At $\Sigma = 3.25$, there are two bifurcation points: at $\Lambda = 0.4$ and $\Lambda = 2.65$.

Hence for fixed $\Sigma = 3.25$, we have an unstable system for $\Lambda < 0.4$ and $\Lambda > 2.65$, and a stable system for $0.4 < \Lambda < 2.65$. Note that the linear analysis predicts a frequency increase across the two bifurcations.

5.5 Double bifurcation phenomenon

This double bifurcation phenomenon is explored further in Figure 9, in which three simulations of the nonlinear Oldroyd-B model are displayed, each from a different stability regime. We see growing oscillations in Figure 9(a), when we have a low fluid relaxation time which closely resembles a viscous fluid. Increasing the fluid relaxation time causes the oscillations stabilize to a horizontal filament as shown in Figure 9(b). Further increasing Λ results in an unstable system with growing, sustained oscillations, as shown in Figure 9(c). Note that while we have an oscillating filament in both figures 9(a) and (c), the oscillatory behavior changes as we cross the double bifurcation point. For low Λ values, we see high amplitude, low frequency oscillations, while the opposite is true for high Λ values.

This relationship persists across a range of polymer viscosity ratios, as shown in Figure 10. Focusing on a single β value, we can see that the amplitude decreases as we cross the stable region, while frequency

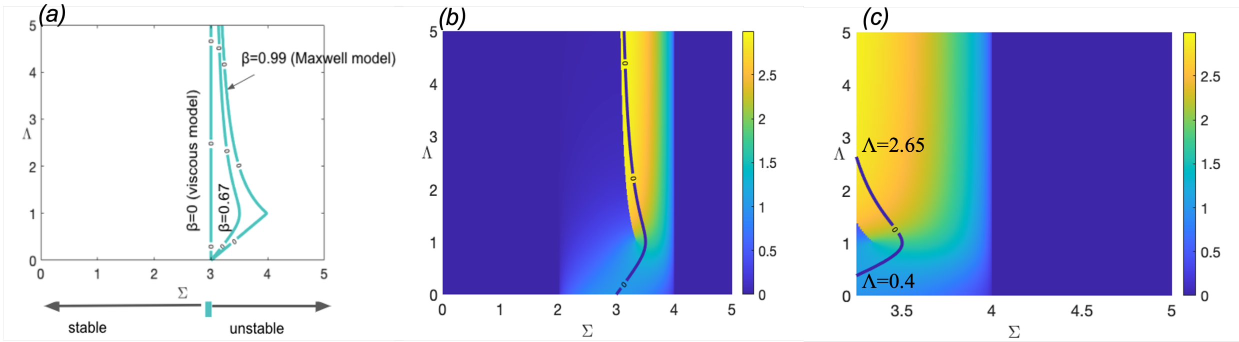

Figure 8: (a) Hopf Bifurcation curve for specified beta values. (b) Bifurcation curve for $\beta = 0.67$, overlaid with frequency prediction from linear analysis. (c) Plot (b) for $\Sigma \geq 3.25$.

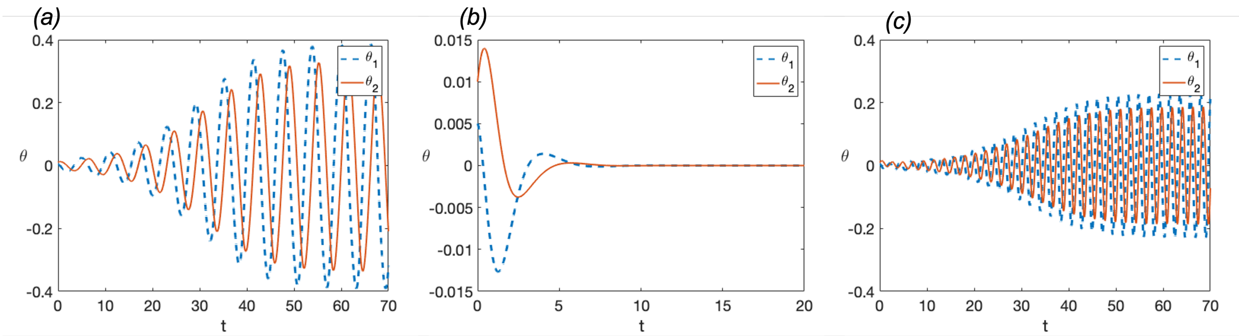

Figure 9: Change in θ_1 and θ_2 for a nonlinear Oldroyd-B two-link filament model. $\beta = 0.67$, $\Sigma = 3.25$. (a) $\Lambda = 0.25$. (b) $\Lambda = 1$. (c) $\Lambda = 3$.

increases. Moreover, looking at the whole range of β values, the amplitude decreases with increasing the polymer viscosity ratio, while the frequency increases. It is also important to note that higher β values result in a longer period of stability across Λ values. In other words, we have to increase the fluid relaxation time further to see emergent oscillations for higher polymer viscosity ratios.

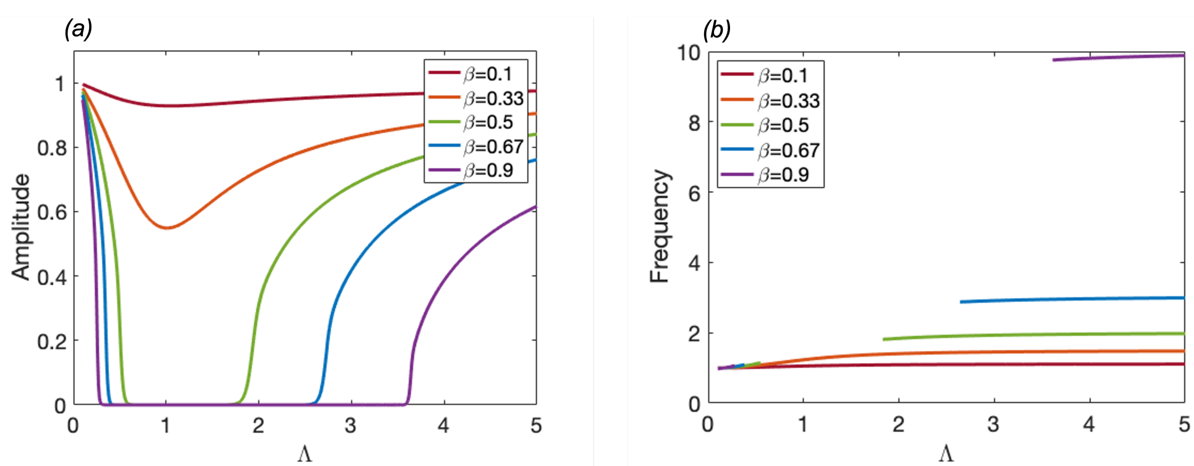

Figure 10: Amplitude and frequency of a nonlinear Oldroyd-B model as a function of Λ, for fixed $\Sigma = 3.25$. The inverse relationship between frequency and amplitude is seen for a range of β values.

5.6 Path classification

In biology, swimmers aren't restricted to one type of motion. Swimming gait varies across organism, environment, and situation. The Oldroyd-B model captures this adaptive nature in its producibility of heterogeneous behavior.

This is exemplified in Figure 11(b), in which the path tracings of the free end of of the two-link model are shown for four different regimes with varying follower forces and fluid relaxation times. These distinct regimes can be seen in Figure 11(a), from the amplitude and frequency extraction from the nonlinear Oldroyd-B model with $\beta = 0.67$. Different Σ and Λ values can result in drastically different behavior.

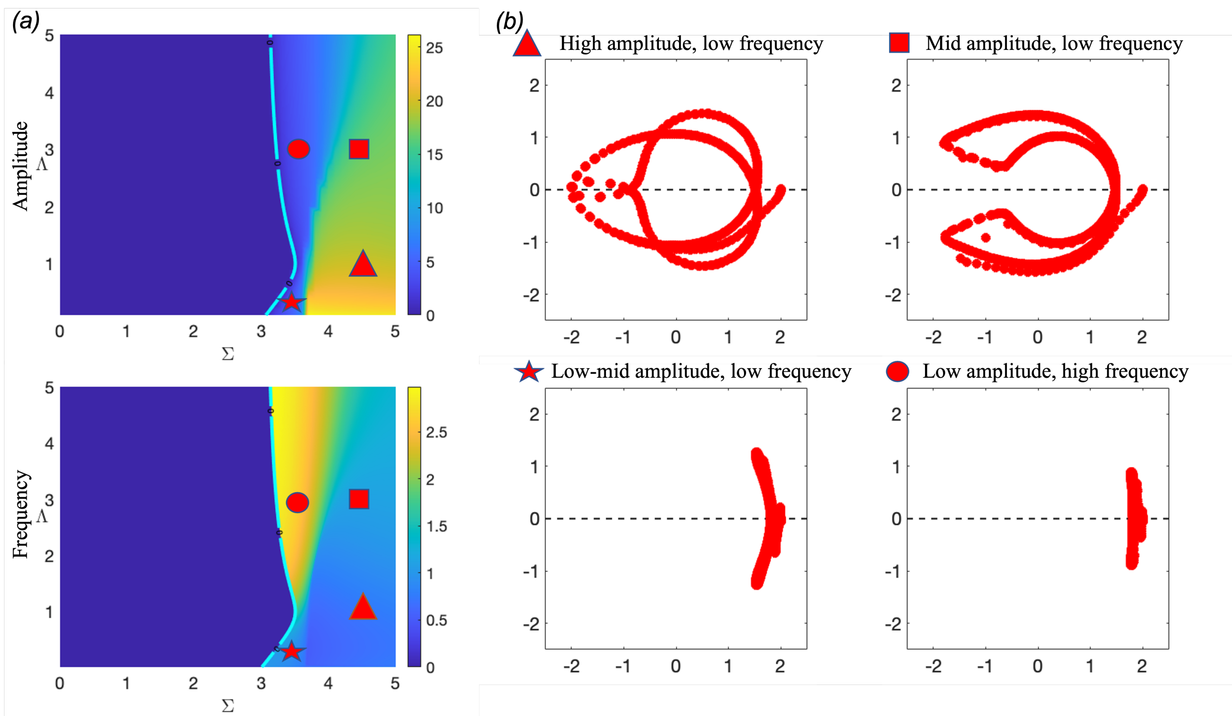

Figure 11: (a) Amplitude and frequency extracted from the nonlinear Oldroyd-B model, over a range of Σ and Λ values, with fixed $\beta = 0.67$. Overlaid with the Hopf bifurcation curve from the linear stability analysis. (b) Path tracings of the free end (point B) of the two-link model for the specified follower force and viscoelasticity regimes.

The bottom two path tracings (star, circle) represent what we may consider a more "familiar" motion with simple oscillations. A strength of this model is that this is not the sole producible behavior. The top two path tracings (triangle, square) highlight this behavioral diversity by representing a "whipping" motion in which the filament rotates past its point of origin. This encompasses the adaptability of microorganisms to different fluid environments.

6 Conclusion

We have explored three different fluid models to classify the oscillatory motion of a two-link model of a flagellum/cilium generated by a tangential follower force. Inspired by *DeCanio et al.*, We began with a viscous fluid model, in which we considered the emergence of oscillations as a function of follower force strength. There is a point at which the magnitude of this force is large enough to cause the filament to buckle, allowing for self-sustained oscillations, represented by the Hopf bifurcation point of the system.

Accounting for the fact that many biological swimmers don't live in purely viscous fluids, we went on to consider models of viscoelastic fluids. The first such model was the Maxwell model. A new parameter was introduced to represent the elasticity of the fluid– or how long it took for the fluid to revert to its original state once it was deformed. We saw that increasing fluid elasticity dampens oscillations, thus increasing the follower force required for sustained oscillations to occur. Linear stability analysis allowed for us to solve for the Hopf bifurcation curve of this system: a linear relationship between the folower force strength and fluid relaxation time. While this model allowed for analysis and insight into the effect of viscoelasticity, it was limited by the follower force strength and did not allow for a smooth transistion from the viscous model.

Taking these shortcomings into consideration, we derived an Oldroyd-B fluid model, adding a fluid viscous term to our system. This presented a new parameter that allowed us to modify the degree of viscoelasticity of the fluid, so that we could smoothly transition from a purely viscous fluid to a purely elastic fluid. In low elasticity regimes, we saw reconciliation with the Maxwell model, in that viscoelasticity can stabilize and dampen oscillations. However, as we increased fluid relaxation time further, a second bifurcation point was found for some follower force strengths, in which the reemergence of oscillations was observed. Across this second bifurcation point, we saw an inverse relationship between amplitude and frequency. This was consistent across different polymer viscosity ratios as well, allowing us to conclude that increasing fluid viscoelasticity decreases oscillatory amplitude while increasing its frequency. The adaptability of swimmers to different environments was highlighted by the heterogeneity of producible behaviors based on the follower force strength and fluid viscoelasticity. Both "simple" oscillations and "whipping" motion were observed.

There are many directions we could take this work to better understand the effect of viscoelasticity on flagellar motion. Adding more links to the model would allow for a gradual progression towards a continuous filament model, more consistent with the structure of an actual flagellum/cilium. In many situations, swimmers do not have just one flagella or cilia that propels the organism. For instance, many cilia line the lungs that coordinate movement with one another. Thus, adding multiple filaments side-by-side would allow us to explore the effect of proximity to beat coordination. Finally, exploring other models of viscoelastic fluids would help to understand other possible effects that viscoelasticity has on locomotion.

7 Acknowledgements

I would like to thank Katie Link, Bob Guy, and Becca Thomases for their continued support and mentorship. Their expertise and excitement about math has made this project enjoyable, and I have learned so much from them. I would also like to thank Michaela Rapier and Corey Beck for their collaboration throughout this project. I would like to thank Greg Kuperberg, Javier Arsuaga, and Jenny Brown for making this REU possible. And finally, I would like to thank the other REU participants for making this summer truly memorable.

References

[1] Gabriele De Canio, Eric Lauga, and Raymond E. Goldstein. Spontaneous oscillations of elastic filaments induced by molecular motors. *Journal of the Royal Society Interface*, 14.136:1–11, 2017. 20170491.

[2] Edward M. Purcell. Life at low reynolds number. *American Journal of Physics*, 45.1:3–11, 1977.

[3] Joseph Teran, Lisa Fauci, and Michael Shelley. Viscoelastic fluid response can increase the speed and efficiency of a free swimmer. *Phys. Rev. Lett.*, 104:038101 (1–4), 2010.